

Supporting information

Constructing a Gradient Soft-Coupled SEI Film via a Dilute Ternary

Electrolyte System towards High-Performance Zinc-Ion Batteries

with Wide Temperature Stability

Tiantian Wang^{a, c}, Yuao Wang^{b, c}, Peng Cui^a, Heshun Geng^a, Yusheng wu^a,

Fang Hu^{a*} Junhua You^{a*} Kai Zhu^{b*}

^aSchool of Materials Science and Engineering, Shenyang University of
Technology, Shenyang 110870, Liaoning, China

^b Key Laboratory of Superlight Materials and Surface Technology of Ministry
of Education, College of Materials Science and Chemical Engineering, Harbin
Engineering University, Harbin 150010, Heilongjiang, China

^cThese authors contributed equally: Tiantian Wang, Yuao Wang

E-mail: hufang25@126.com

Experiments

Synthesis of W-VO₂:

Materials preparation: The W-VO₂ was prepared with a simple solvothermal method. The Solvothermal solution was prepared by dissolving 0.6g V₂O₅ powder and 1.2g H₂C₂O₄ powder into 20 mL of distilled water at 85 °C for vigorous stirring about 3 h until VOC₂O₄ (dark blue solution) was formed. Then 4.67 mL 30 % H₂O₂ was slowly added (this step reacts violently) and kept continuously stirring about 30 min to obtain a brown solution, then 67 mg (NH₄)₁₀(H₂W₁₂O₄₂)₄H₂O was finally added into above-mentioned solution to obtain the W-doped vanadium oxide solution and stirred for 10 min until it was totally dissolved. The mixture was then given a 60 mL ethanol addition, and stirring continued for 60 min. The created dark-green slurry was then put into a 100 mL Teflon-lined autoclave and heated to 170°C for 12 hours. The precipitate was then collected, carefully cleaned with ethanol and deionized water, and dried for 12 hours at 60°C.

Synthesis of ZnHCF cathode¹: 50 mL of 0.1 M ZnSO₄ and 50 mL 0.05 M K₃Fe(CN)₆ were simultaneously added into 25 mL DI water at 60 °C under vigorous stirring. Afterwards, the orange suspension was stirring for several hours to complete the reaction. The precipitate was rinsed and centrifuged for several times to remove the residues. Then, the product was finally dried at 70 °C overnight. An active electrode was prepared by mixing acetylene black, polytetrafluoroethylene emulsion, and active materials in a weight ratio of 2:1:7. Then upon rolling the mixture into a uniform thickness, which was pressed onto conductive carbon paper with a diameter of 1 cm. The active materials were loaded at an average mass of 5 mg/cm².

Synthesis of NH₄V₄O₁₀ cathode:

0.9356 g of NH₄VO₃ (AR 99.5%) was dissolved in 80 mL of deionized water, heated to 60 °C, and stirred until fully dissolved. Upon returning to room temperature, 1.008 g of H₂C₂O₄·2H₂O (AR 98.0%) was introduced as a reductant. After 0.5 hours of magnetic stirring, the solution distinctly transitioned to a clarified brownish-yellow hue. Ultimately, we put the solution in a 100-mL autoclave, sealed it gradually, and subjected it to a reaction at 180 °C for 6 hours. Subsequently, the precipitate was

gathered when the autoclave temperature was reduced to ambient temperature, washed several times with distilled water and anhydrous ethanol, dried at 60 °C for 24 hours, and designated as NVO.

Synthesis of V_6O_{13} cathode²:

Vanadium oxides nanobelts were prepared by a facile solvothermal method that we reported previously. In a typical process, 0.4 g of V_2O_5 was added to a mixed solution of C_2H_5OH and deionized water (The volume ratio is 5:4, DIW) under strong stirring until the solution was dispersive evenly. The mixed solution was transferred to a 100 mL autoclave, sealed, and kept at 160°C for 24 hours. After cooling to room temperature, the pristine $V_6O_{13} \cdot 2.72H_2O$ products were obtained through centrifugation with DIW and ethanol. Then, pristine $V_6O_{13} \cdot 2.72H_2O$ sample was calcined at 400°C for 1 h with a heating rate of 5°C/min in argon atmosphere to obtain the vanadium oxides ultrathin nanobelts.

Preparation of the electrolytes:

$Zn(OTf)_2$ (0.1 M, 0.3 M, 0.5 M, 1.0 M, 1.5 M) was dissolved in pure H_2O , acetonitrile (AN, C_2H_3N), and dimethyl sulfoxide (DMSO, C_2H_6OS) (the molar ratios of H_2O , DMSO and AN were 2:1:3.5) solvents for 30 min at room temperature with vigorous stirring to form ternary electrolytes with different concentrations named TSIS-0.1, TSIS-0.3, TSIS-0.5, TSIS-1.0, TSIS-1.5. At the same time, $Zn(OTf)_2$ (0.3 M) was dissolved in H_2O and AN (molar ratio is 2:3.5), H_2O and DMSO (molar ratio is 2:1) to form a binary electrolyte named BSIS-A, BSIS-D as a control. In addition, 3 M $Zn(OTf)_2$ as a control.

Materials characterizations

The X-Ray diffraction (XRD) patterns of the samples were collected using a powder X-ray diffractometer (Cu $K\alpha$ radiation source, D8, Bruker). Fourier Transform Infrared (FT-IR) analysis was conducted on Nicolet iS50. Raman spectroscopy was recorded on LabRAM HR Evolution with an excitation wavelength of 633 nm.

Scanning electron microscopy (SEM) images were collected using FEI Microscope (JSM-7900F). Transmission electron microscopy (TEM) and energy dispersive X-ray spectroscopy (EDS) were performed on Talos F200X G2. The compositions of solid electrolyte interphase (SEI) were determined by X-ray photoelectron spectroscopy (XPS, Axis Ultra DLD) using monochromatic 1486.7 X-ray source. The prominent C 1s peak was calibrated to 284.8 eV. In situ optical observation of the zinc anodes was carried out in a transparent cuboid electrolytic cell using an industrial microscope (KYH3800S42, KangYuan Electronic). Differential scanning calorimetry (DSC, METTLER TOLEDO DSC3) was used to measure the freezing point of the hybrid electrolyte at a temperature range from -80 °C to 25 °C, which was carried out in a liquid nitrogen cooling system with a heating rate of 5 °C min⁻¹.

Electrochemical measurements

2032-type coin cells were assembled to measure the Coulombic efficiency and cycling stability of Zn metal anode (100 μm) on a standard battery tester (LAND-CT2001A) at different temperatures controlled by cryostat (-30 °C), fridge (-20 °C), room temperature (25 °C), and oven (40 °C). The separator used was glass fiber (Waterman GF/D). The cycling stability was evaluated in symmetric cells composed of two identical Zn disks in the electrolyte of TSIS-X and 3 M Zn(OTf)₂ at different current densities and capacities. For the measurement of Coulombic efficiency, the coin cells were composed of titanium (Ti) foil as the working electrode (substrate for Zn plating and stripping), and a piece of Zn foil as the counter and reference electrode. A constant current with a constant capacity (the amount of Zn deposited) was applied to the electrode, followed by Zn stripping via charging to 1 V (versus Zn/Zn²⁺). The Coulombic efficiency of each cycle was calculated as the amount of Zn stripped (based on capacity extracted) divided by the amount of Zn plated (based on capacity deposited) onto the Ti foil. Linear sweep voltammetry (LSV) of the hybrid electrolytes was measured using |Zn||Ti asymmetric at a scan rate of 5 mV s⁻¹ in a voltage range of -1 to 4 V (versus Zn/Zn²⁺) on an electrochemical workstation (Ivium-n-Stat, Nederlanden). The ionic conductivity of hybrid electrolytes at different temperatures was measured

by EIS via symmetric cells consisting of two electrodes. The distance between the two electrodes is 1.5 mm, and the applied frequency range was from 10^5 Hz to 10^{-1} Hz with 5 mV AC amplitude. The ionic conductivity of the hybrid electrolyte was calculated by the following equation:

$$\sigma = \frac{L}{R_b S}$$

The following expression describes the relationship between ionic conductivity ($S\text{ cm}^{-1}$), resistance (ohm), and electrode surface area (cm): which corresponds to the intercept of the Nyquist plot. L is the distance between two electrodes (cm). The electrochemical performance of the full cell was evaluated by using both the 2032-type coin cells and pouch cells. For the routine test of the coin-type full cell, the typical mass loading of active materials is around $4\text{--}5\text{ mg cm}^{-2}$, glass fiber (Waterman GF/D) as separator and $100\text{ }\mu\text{m}$ Zn metal as anode. The electrolyte was fixed to around $130\text{ }\mu\text{L}$. The galvanostatic discharge/charge tests were performed using LAND-CT2001A instruments. Electrochemical impedance spectroscopy (EIS) measurements were carried out on an electrochemical workstation (Ivium-n-Stat, Nederlanden) from 10^5 Hz to 10^{-1} Hz , and the perturbation amplitude was 5 mV. All the tests at different temperatures were carried out after 4 h of resting.

Computational details

To obtain the HOMO and LUMO energy levels, we performed density functional theory (DFT) calculations. All calculations were carried out using DMol³ program^{1,2}. Becke three parameter hybrid functional combined with the Lee-Yang-Parr correlation (B3LYP) functional^{3,4} was used for the exchange correlation energy. Spin-polarized calculations were adopted for all model systems and van der Waals correction was also considered by implementing the Tkatchenko-Scheffler (TS) method⁵. All electron relativistic core treatment and 4.4 version of the double numerical plus polarization (DNP) basis set were used to describe the core electrons and the atomic orbital basis set, respectively. The convergence criteria for the geometry optimization were 10^{-5} Ha for energy, $0.002\text{ Ha}/\text{\AA}$ for force, and 0.005 \AA for displacement. The self-consistent

field convergence was less than 1.0×10^{-6} Ha. The simulation system studied in this paper contained the polyelectrolyte molecules: metal cations (Zn^{2+}), OTf^- , H_2O , DMSO and AN molecule. It represented the organic-inorganic hybrid system, and the COMPASS force field could provide the precise atomic parameters for polyelectrolyte molecules, inorganic ions, and water molecules. Prior studies have demonstrated the applicability of the COMPASS force field to such organic-inorganic hybrid systems^{3 4 5}. The newly added COMPASSIII force field in Materials Studio software enhances the support of polymers systems on the basis of the COMPASS force field. Therefore, the COMPASSIII force field was selected for this study. The ESP charge was used for all components. The MD simulations were carried out using cubic cells with a linear dimension of for $\text{Zn}(\text{OTf})_2\text{-H}_2\text{O}$ (containing 150 $\text{Zn}(\text{OTf})_2$ and 2700 H_2O), TSIS-0.1 (containing 12 $\text{Zn}(\text{OTf})_2$, 1575 AN, 450 DMSO and 900 H_2O), TSIS-0.3 (containing 40 $\text{Zn}(\text{OTf})_2$, 1680 AN, 480 DMSO and 960 H_2O), TSIS-0.5 (containing 42 $\text{Zn}(\text{OTf})_2$, 1050 AN, 300 DMSO and 600 H_2O), TSIS-1.0 (containing 85 $\text{Zn}(\text{OTf})_2$, 1050 AN, 300 DMSO and 600 H_2O) and TSIS-1.5 (containing 127 $\text{Zn}(\text{OTf})_2$, 1050 AN, 300 DMSO and 600 H_2O), using the Amorphous cell module to establish a cube with periodic boundary conditions. The temperature was set to be constant at 298 K, and the highest convergence accuracy was selected (Ultra-fine). The system maintained electrical neutrality. After the AC simulation box was built, the Forcite module was used for geometry optimization. MDSs were performed using the Forcite module in Materials Studio software. First, the Conjugate gradient was chosen to geometrically optimize the initial structure of the system. Next, dynamic equilibrium (Dynamics) was performed on the NPT ensemble ($P = 0.0001$ Gpa, $T = 298$ K) to obtain a stable system density with a simulation time of 1500 ps. For the last frame structure obtained by the NPT ensemble under the equilibrium process, the molecules of the polyelectrolyte chain were fixed using Constraints under the Modify toolbar, and the ions to be analyzed were designated as set, followed by the NVT ensemble (regular ensemble) for dynamic equilibrium. The total simulation time under the NVT ensemble was 1 ns for system sampling analysis. In all dynamic simulations, the initial velocity of the atoms in the system was randomly assigned by the Boltzmann distribution at a given temperature;

the non-bonded interaction energy had a truncation radius of 20 Å, and the summation method was Atom Based. The method of summing up the coulomb electrostatic potential energy was Particle Particle-Particle Mesh (PPPM), which could increase the speed of the large system Ewald and improve the computational efficiency when dealing with large-scale charged systems. The Berendsen constant temperature thermal bath method was selected for the temperature control, and the Berendsen constant pressure device was selected for the pressure control.

To provide a more complete description of the electrolyte considered in this study, the transport properties of Zinc ions in electrolyte were also calculated from MD simulations. The simulations were run using an NPT ensemble during 1000 ps with a time step of 100 fs at 298 K. This methodology has commonly been used to successfully estimate diffusion coefficients of SSEs. First, the diffusivity (D) of Zinc ions was determined at 298 K from the Einstein relation, where $n = 3$ is the dimension of the system, $MSD(\Delta t)$ is the mean squared displacement of Zn ions over the time interval Δt . We go to the 500 steps where the diffusion coefficient varies within 10% to calculate its ionic conductivity. The MSD was computed using Materials Studio ⁶.

$$D = \frac{1}{2n} \frac{MSD(\Delta t)}{\Delta t}$$

where n represents the density of the particles, e represents charge, D represents diffusion coefficient, k_B represents Boltzmann's constant, T represents temperature.

Interaction energy. The interaction energy represents the energy released by small particles when they are combined into larger particles or the energy generated during the adsorption process. The larger the value, the stronger the interaction between the small particles and the system. For the A + B system, the interaction energy ΔE is calculated by the following formula:

$$\Delta E = E_{AB} - (E_A + E_B)$$

where E_{AB} is the total energy of the system, E_A is the energy of substance A, and E_B is the energy of substance B.

Adsorption energy (E_a) calculations. Density functional theory (DFT) calculations were carried out using the projector-augmented wave (PAW) method as implemented

in the Vienna ab initio simulation package (VASP) ^{7 8}. A generalized gradient approximation (GGA) of Perdew–Burke– Ernzerhof (PBE) functional was employed to describe the exchange-correlation interaction ⁹. An energy cutoff of 450 eV and Gamma-centered $3 \times 3 \times 1$ k-points mesh were applied to all calculations. To explore the interactions between a Zn atom and substrates (Zn (002), ZnF₂ (020), ZnS(106), Zn(N₃)₂(012)) cleaved from the corresponding crystal structure as the most stable surface, and a vacuum layer of 20 Å was adopted. The structures were relaxed until the forces and total energy on all atoms were converged to less than 0.01 eV Å⁻¹ and 1×10^{-5} eV, respectively. Visualization of the structures is made by using VESTA software. Here, E_a was calculated by the energy difference of the system after and before adsorption ¹⁰:

$$E_a = E_{Zn-substrate} - 1/2E_{Zn2} - E_{substrate}$$

where $E_{Zn-substrate}$, $1/2E_{Zn2}$, and $E_{substrate}$ represent the energies of the Zn adsorbed metal surface, Zn atom, and the clean metal surface, respectively.

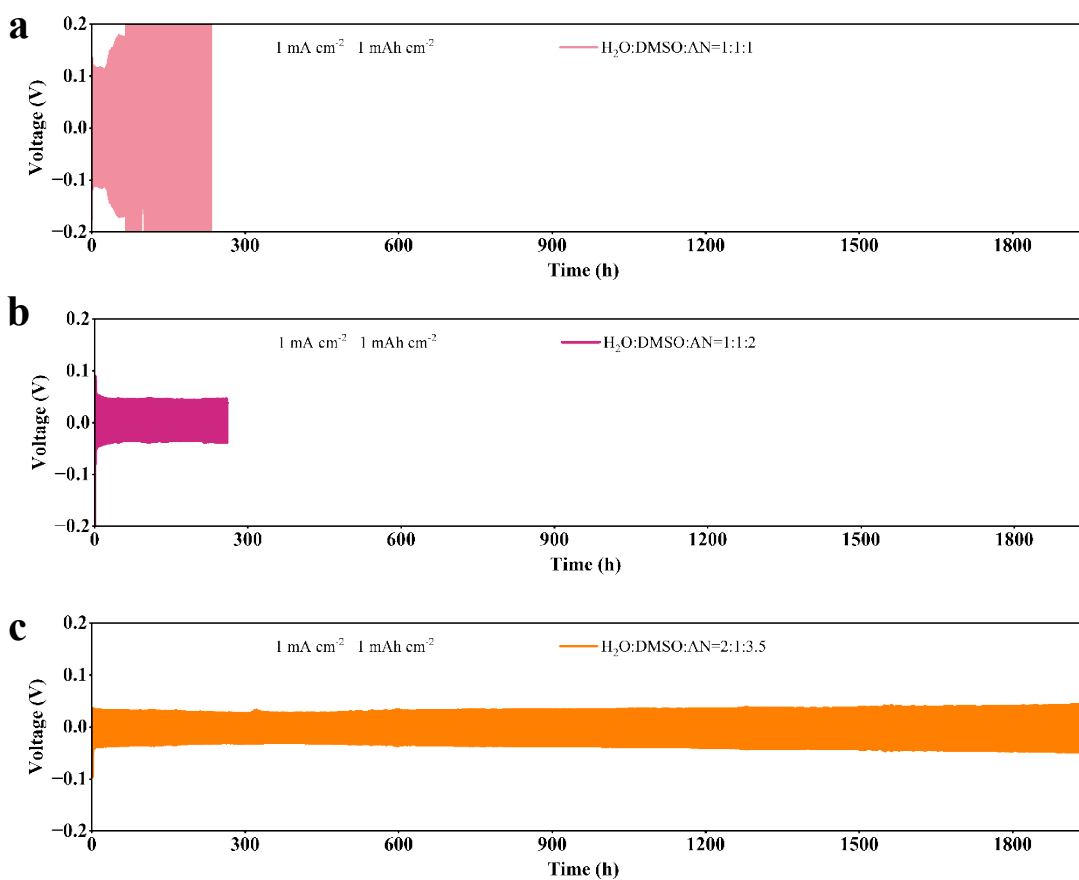


Fig.S1. (a-c) The voltage profiles of the Zn||Zn symmetric cell tested in different electrolyte (The molar ratio of H₂O:DMSO:AN is 1:1:1, 1:1:2, 2:1:3.5) at the current density of 1 mA cm^{-2} with the capacity of 1 mA h cm^{-2} .

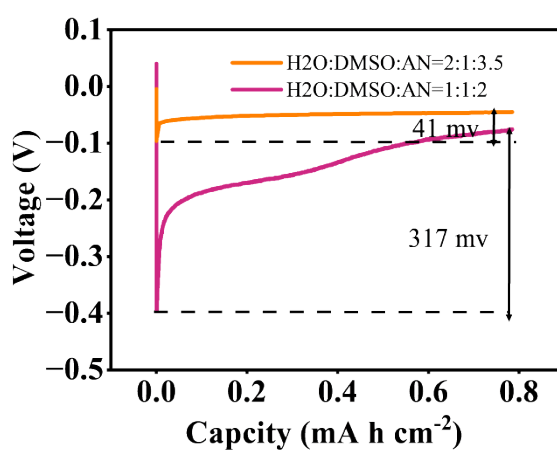


Fig.S2. Nucleation overpotentials in the molar ratio of H₂O: DMSO: AN is 1:1:2 and 2:1:3.5 electrolytes at 1st cycle.

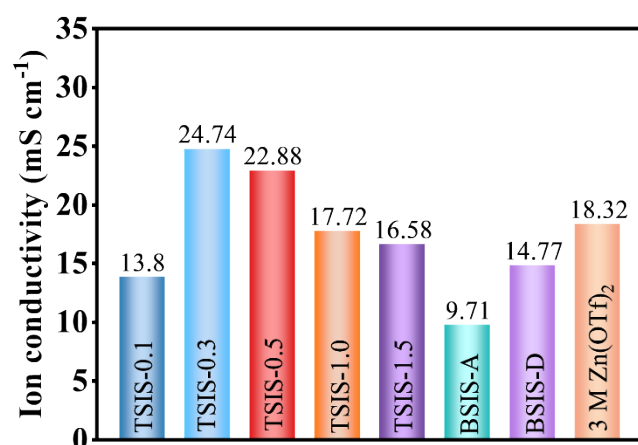


Fig.S3. Ionic conductivity of the 3 M Zn(OTf)₂, TSIS-0.1, TSIS-0.3, TSIS-0.5, TSIS-1.0, TSIS-1.5, BSIS-D, BSIS-A electrolytes.

The following expression describes the relationship between ionic conductivity (mS cm⁻¹), resistance (ohm), and electrode surface area (cm²):

$$\sigma = \frac{L}{R_b S}$$

where σ is ionic conductivity, R is ionic resistance, L is the inter-electrode distance between voltage-sensing electrodes, and S is the electrode surface area normal to current flow. In a typical Nyquist plot, extrapolation of a semi-circle arc or low-frequency linear spectra to the X-axis gives the ionic resistance ¹¹.

Table S1. Ion conductivity

	R_b	$L(\text{cm})$	$S(\text{cm}^2)$	$\sigma(\text{mS cm}^{-1})$
TSIS-0.1	7.02	0.15	1.5386	13.88
TSIS-0.3	3.94	0.15	1.5386	24.74
TSIS-0.5	4.26	0.15	1.5386	22.88
TSIS-1.0	5.5	0.15	1.5386	17.72
TSIS-1.5	5.88	0.15	1.5386	16.58
BSIS-D	10.04	0.15	1.5386	9.71
BSIS-A	6.6	0.15	1.5386	14.77
3 M Zn(OTf) ₂	5.32	0.15	1.5386	18.35



Fig.S4. The optical photographs of the 3 M Zn(OTf)₂, TSIS-0.1, TSIS-0.3, TSIS-0.5, TSIS-1.0, TSIS-1.5, BSIS-D, BSIS-A electrolytes.

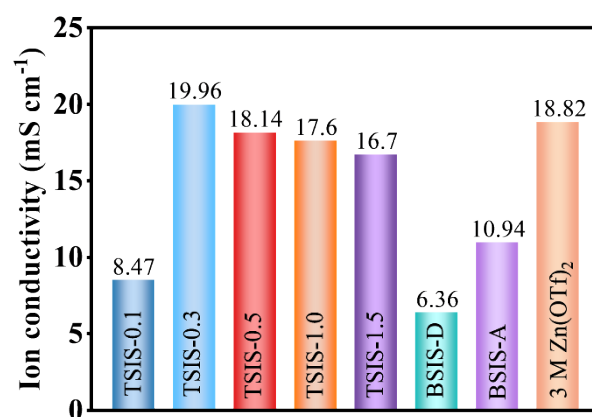


Fig.S5. Ionic conductivity of the 3 M Zn(OTf)₂, TSIS-0.1, TSIS-0.3, TSIS-0.5, TSIS-1.0, TSIS-1.5, BSIS-D, BSIS-A electrolytes.

Table S2. Diffusion coefficients of different electrolytes

TSIS-0.3										
	1-2001	1001-3001	2001-4001	3001-5001	4001-6001	5001-7001	6001-8001	7001-9001	8001-10001	
Diffusion coefficient (A ² /ps)	0.3098	0.3190	0.3146	0.3242	0.3300	0.3343	0.3379	0.3305	0.3248	
R ²	1	1	1	1	1	1	1	1	1	
Zn ²⁺ diffusion coefficient (A ² /ps)							6.759×10 ⁻²			

BSIS-D										
	1-2001	1001-3001	2001-4001	3001-5001	4001-6001	5001-7001	6001-8001	7001-9001	8001-10001	
Diffusion coefficient (A ² /ps)	0.2565	0.2600	0.2713	0.2664	0.2671	0.259	0.2622	0.2671	0.2743	
R ²	1	1	0.9999	1	1	1	1	1	1	
Zn ²⁺ diffusion coefficient (A ² /ps)							3.947×10 ⁻²			

BSIS-A										
	1-2001	1001-3001	2001-4001	3001-5001	4001-6001	5001-7001	6001-8001	7001-9001	8001-10001	
Diffusion coefficient (A ² /ps)	0.285	0.2892	0.3055	0.3144	0.3230	0.3162	0.3183	0.3174	0.3180	
R ²	1	1	1	1	1	0.9999	1	1	1	
Zn ²⁺ diffusion coefficient (A ² /ps)							5.854×10 ⁻²			

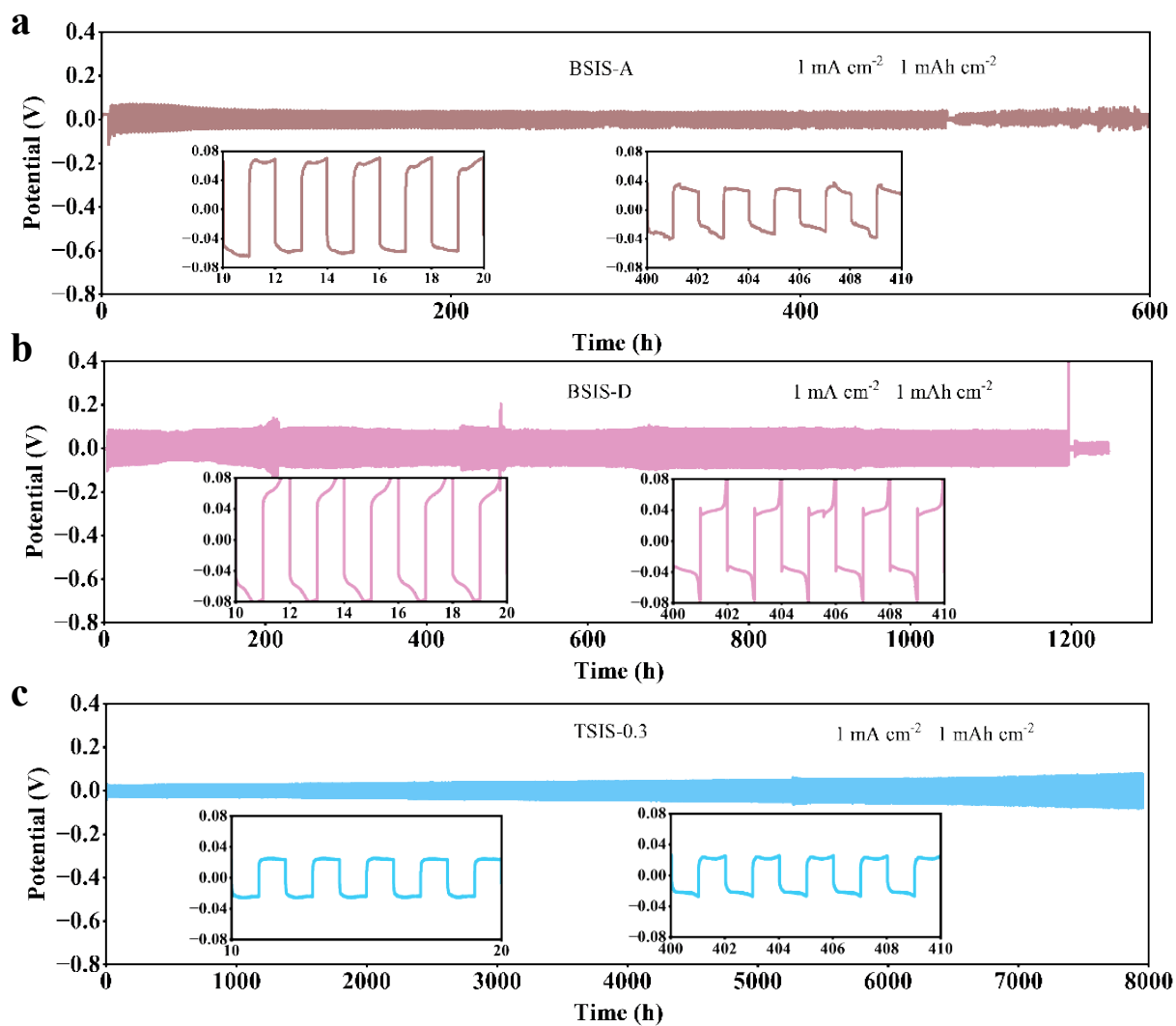


Fig.S6. The voltage profiles of the Zn||Zn symmetric cell tested in different electrolyte (a) BSIS-A, (b)BSIS-D, (c)TSIS-0.3 at the current density of 1 mA cm^{-2} with the capacity of 1 mA h cm^{-2} .

Table S3. Corresponding coordination numbers for the BSIS-A and BSIS-D electrolytes

	TSIS-0.3	BSIS-A	BSIS-D
Zn-OTf ⁻	1.31	1.38	0.2
Zn-AN	0.95	1.54	
Zn-DMSO	0.8		0.99
Zn-H ₂ O	2.73	3.17	4.86

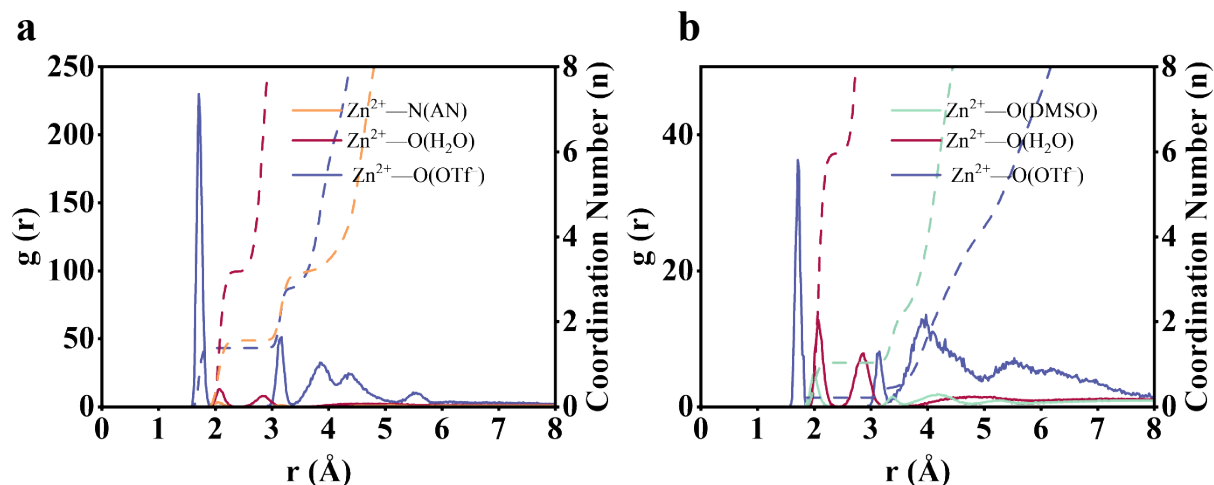


Fig.S7. (a) and (b) RDFs and corresponding coordination numbers for the BSIS-A and BSIS-D electrolytes.

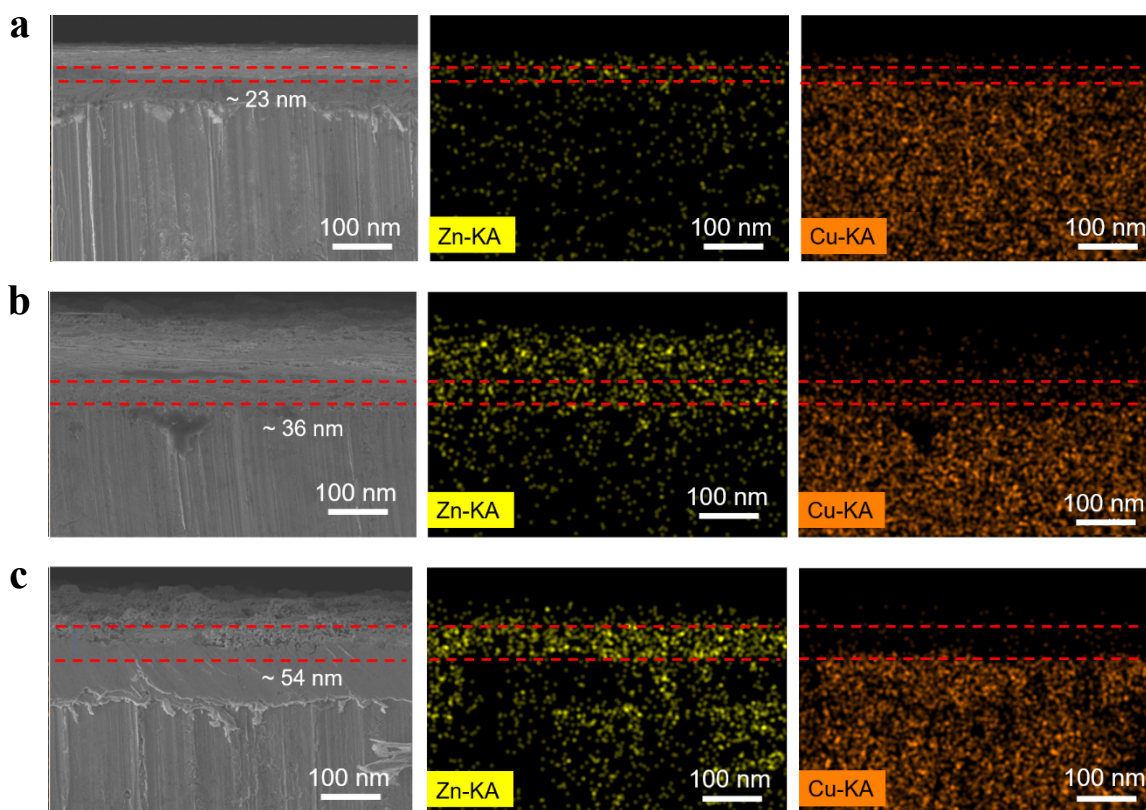


Fig.S8. cross-section SEM images of the Zn anode after 100 cycles for (a), BSIS-D (b) TSIS-0.3 (c) BSIS-A.

Compared to the binary electrolyte, the ternary electrolyte showed larger ionic conductivity, higher ion diffusion coefficient, smaller hysteresis voltage and higher cycle life. At the same time, the addition of DMSO alone at ultra-low concentrations

cannot enable OTf^- enter the first solvated shell layer. The structures of SEI films in the three electrolytes were further carefully characterized using surface and cross-sectional scanning electron microscopy (SEM), and the SEM cross-sectional images showed that the BSIS-D electrolyte formed a very dense and homogeneous SEI layer on the Cu substrate, with a thickness of about 23 nm. The BSIS-A electrolyte had a thick Zn-metal deposit layer on the Cu substrate, and had a porous morphology in some areas, with a SEI thickness of about 54 nm. TSIS-0.3 electrolyte has a porous morphology with smaller particle size and therefore the corresponding Zn and Cu elemental spectra of SEI show that the thickness of SEI is 36 nm (Figure S8). The primary solvated shell layer in the binary BSIS-D electrolyte mainly consists of DMSO and H_2O . DMSO possesses a lower LUMO value than H_2O , thereby inhibiting water decomposition during the zinc deposition process. In addition, DMSO exhibits remarkable zincophilicity, facilitating the rapid and uniform deposition of zinc ions, hence enhancing the cycle life of zinc-ion batteries. AN and OTf^- in the binary BSIS-A simultaneously entered the first solvation shell and exhibited a greater concentration of AN and OTf^- within this shell compared to the ternary TSIS-0.3. The HOMO and LUMO energy level chart indicates that $\text{Zn}(\text{OTf})^+$ and $\text{Zn}(\text{AN})^{2+}$ possess lower LUMO values, perhaps resulting in a thicker SEI layer of BSIS-A during zinc ion deposition (Figure 3a, Tables S3 and Figure S7).

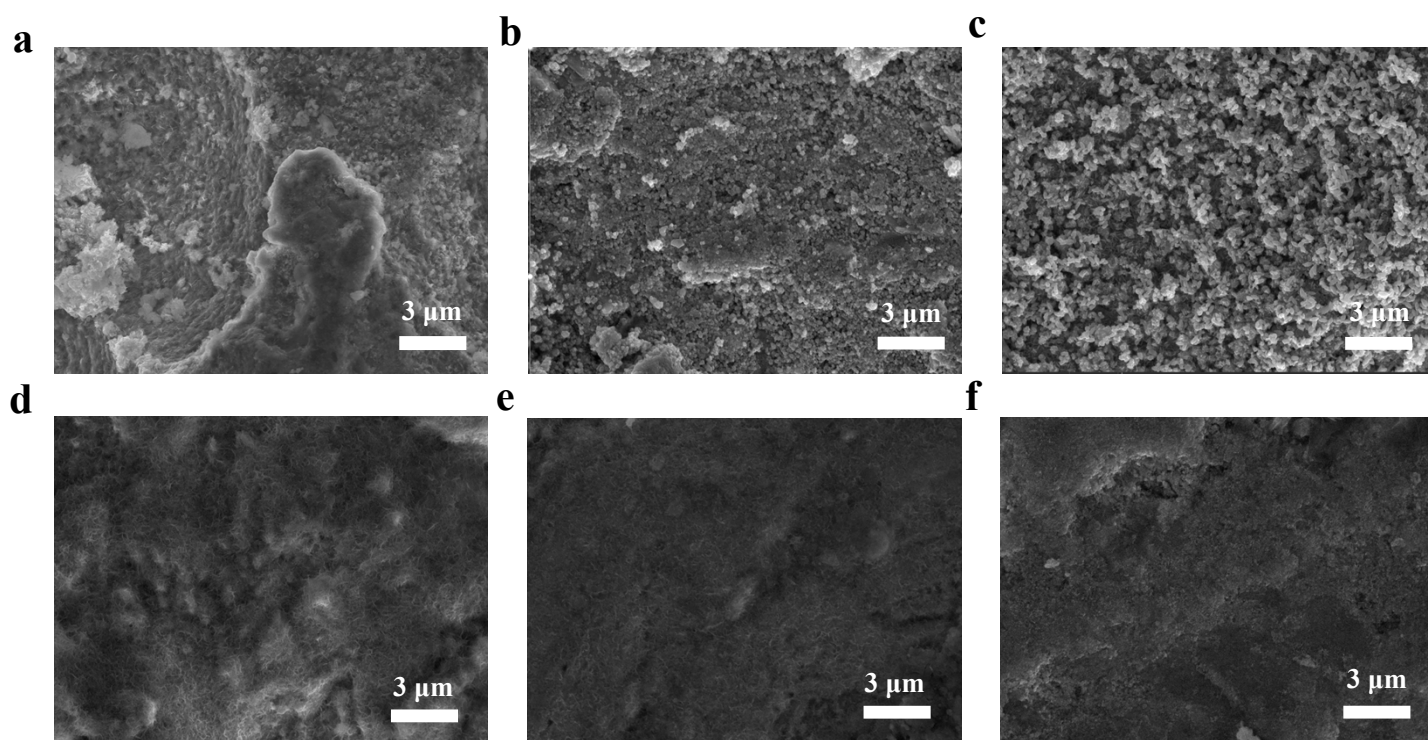


Fig.S9. Top-view SEM images of the Zn anode after 100 cycles for 3M Zn(OTf)₂ (a), TSIS-0.1(b), TSIS-0.3(c), TSIS-0.5(d), TSIS-1.0(e), TSIS-1.5(f) electrolytes.

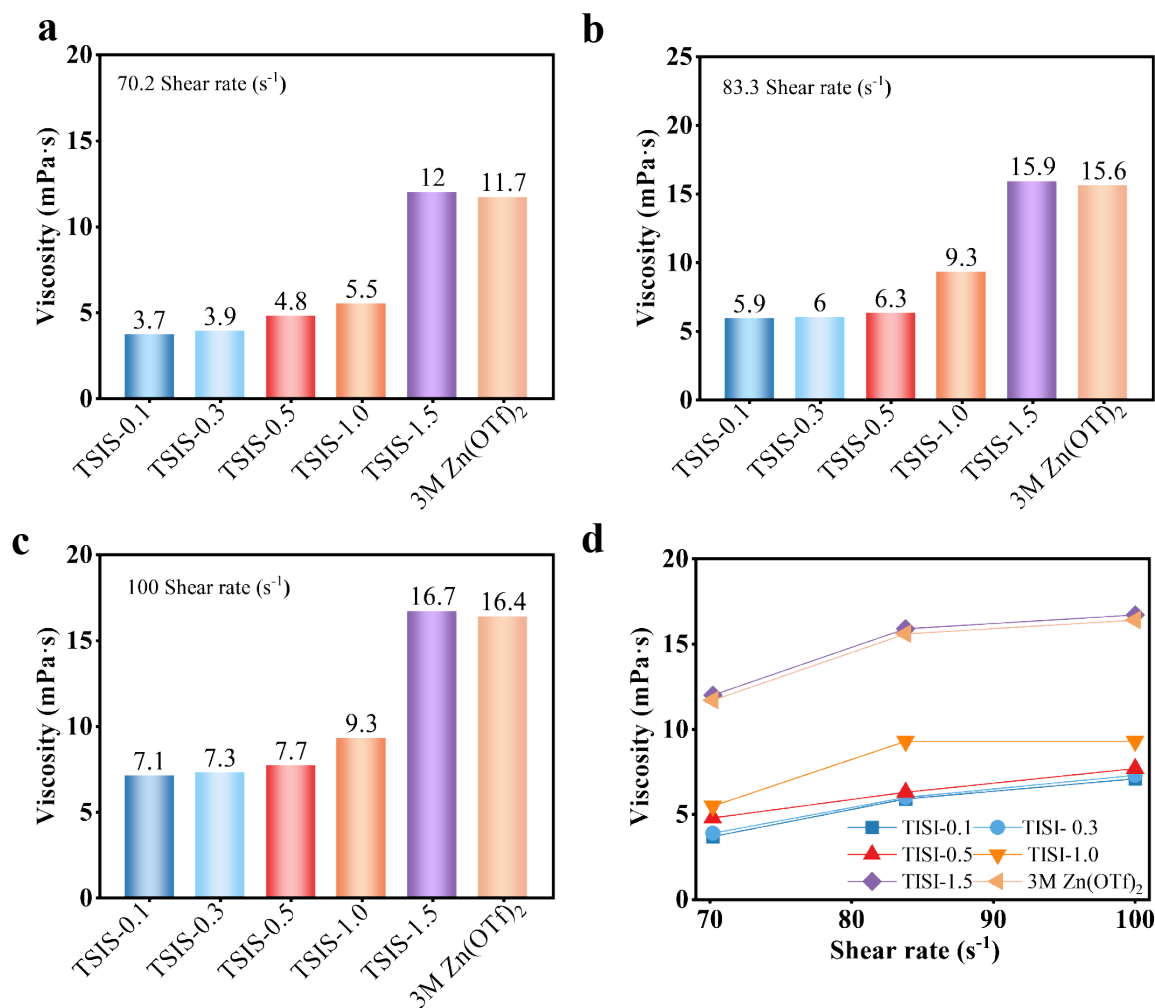


Fig.S10. Viscosity of different electrolytes.

The viscosity of the fluid progressively rises with increasing electrolyte content. At a shear rate of 70.2 S^{-1} , the viscosities are as follows: for TSIS-0.1, 3.7 mPa S ; for TSIS-0.3, 3.9 mPa s ; for TSIS-0.5, 4.8 mPa s ; for TSIS-1.0, 5.5 mPa s ; for TSIS-1.5, 12 mPa s ; and for 3 M Zn(OTf)_2 , 11.7 mPa s . The results indicate that when electrolyte concentration rises, the viscosity of the electrolyte also increases; nevertheless, the concentration of 3 M Zn(OTf)_2 is somewhat lower than that of TSIS-1.5. The viscosity trend of various electrolytes stays consistent with a shear rate of 70.2 S^{-1} . The viscosity of TSIS-0.3 is significantly lower than that of the standard 3 M Zn(OTf)_2 .

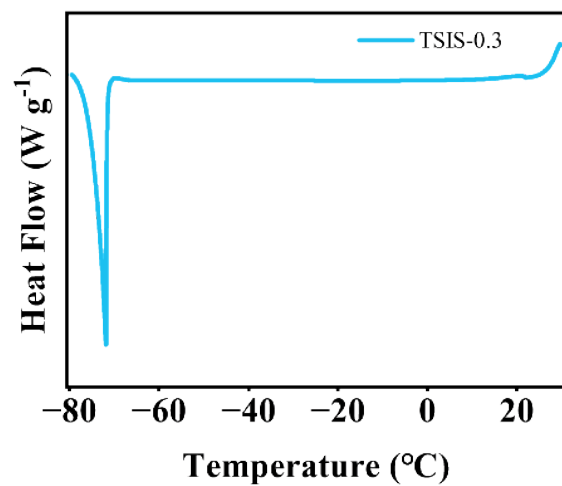


Fig.S11. Differential scanning calorimetry (DSC) curves of TSIS-0.3 electrolytes.

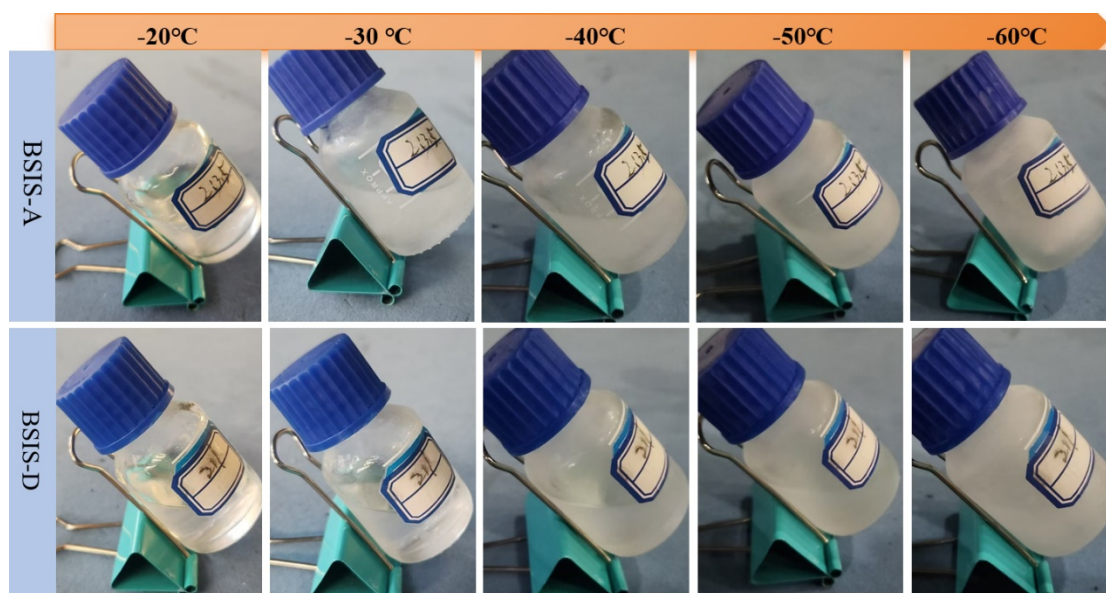


Fig.S12. The optical photographs of the BSIS-A and BSIS-D electrolyte at -20 °C, -30 °C, -40 °C, -50 °C and -60 °C.



Fig.S13. Optical photographs of the BSIS-A and BSIS-D electrolytes after being removed from the instrument at -60°C for 5 minutes at room temperature.

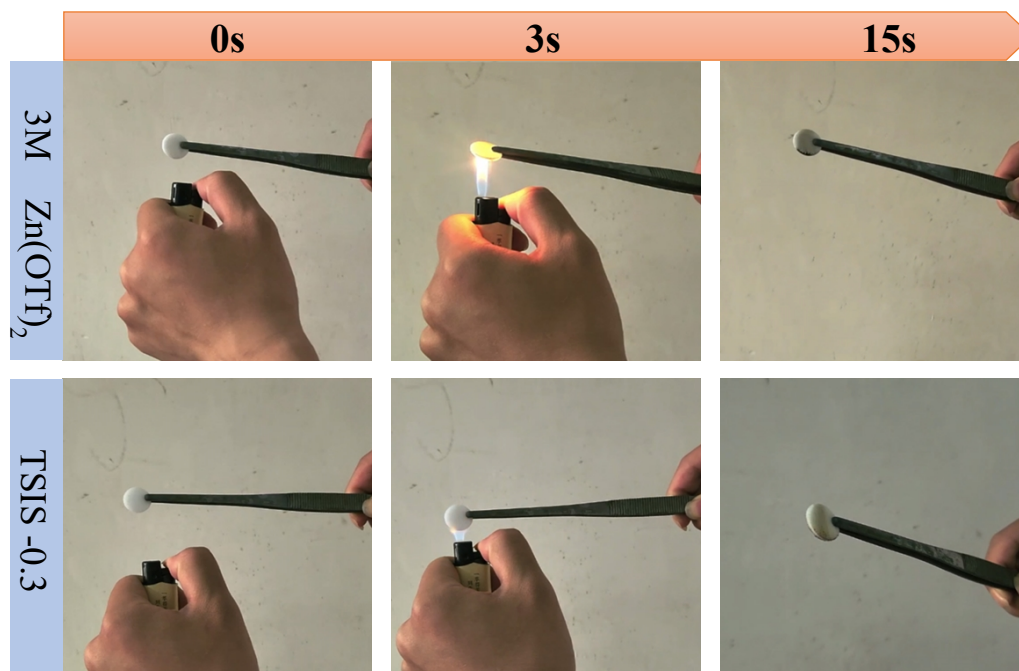


Fig.S14. Photographs of the combustion tests of glass fiber rinsed with 3M $\text{Zn}(\text{OTf})_2$ (top) and TSIS-0.3 (bottom) electrolytes.

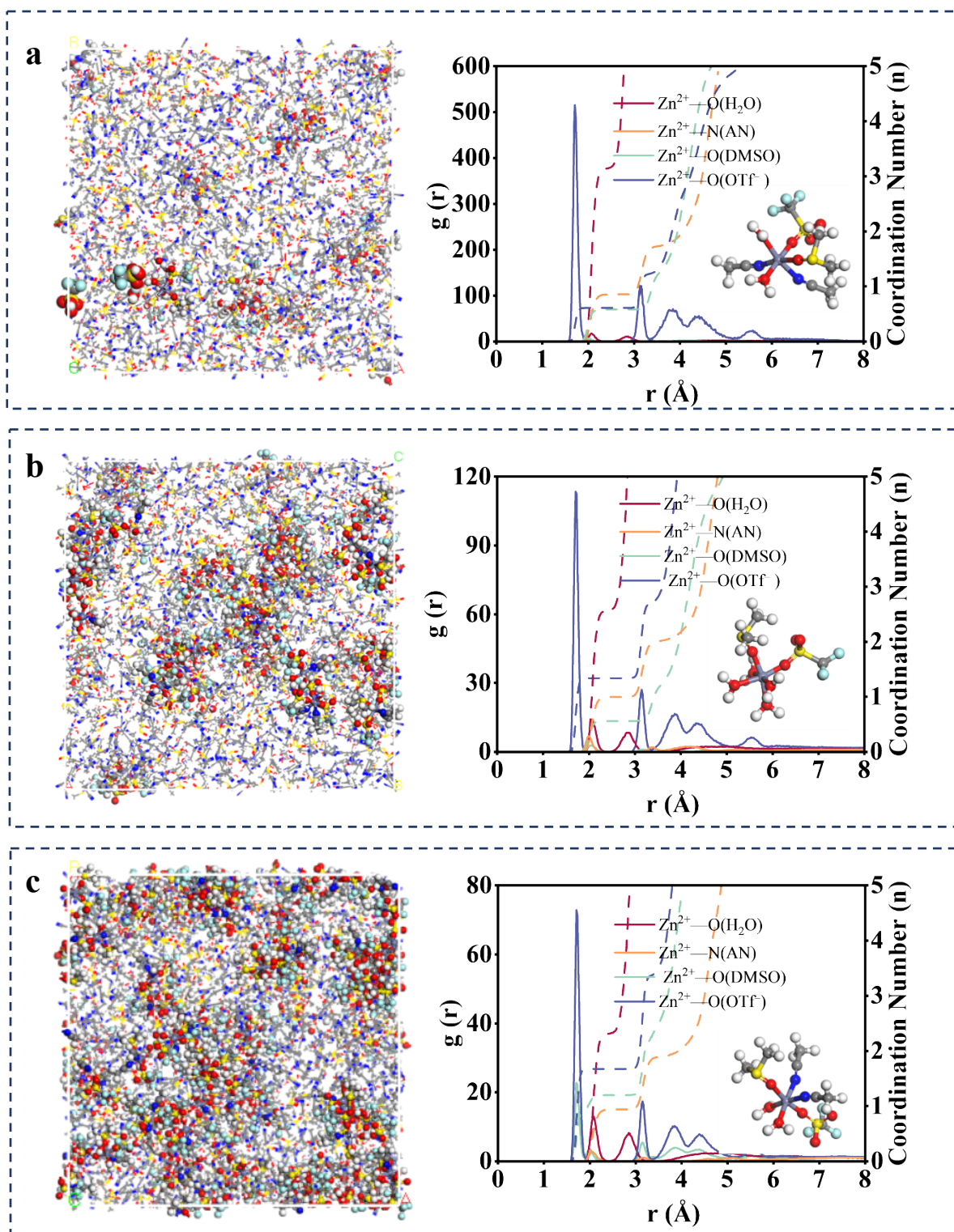


Fig.S15. Physical properties and Zn²⁺ ions coordination structure in electrolytes of the electrolyte. Snapshot of TSIS-0.1 (a), TSIS-0.5(b) and TSIS-1.0 (c) by molecular dynamics simulation.

Table S4. Corresponding coordination number of Zn²⁺- OTf⁻, Zn²⁺- AN, Zn²⁺- DM SO, and Zn²⁺- H₂O in the first solvated shell layer

	0.1	0.3	0.5	1.0	1.5	3 M Zn(OTf) ₂
Zn-OTf ⁻	0.61	1.31	1.34	1.67	1.9	0.8
Zn-AN	1.00	0.95	1.1	1.2	0.9	
Zn-DMSO	0.86	0.8	0.66	0.904	0.75	
Zn-H ₂ O	3.2	2.73	2.7	2.15	2.05	5

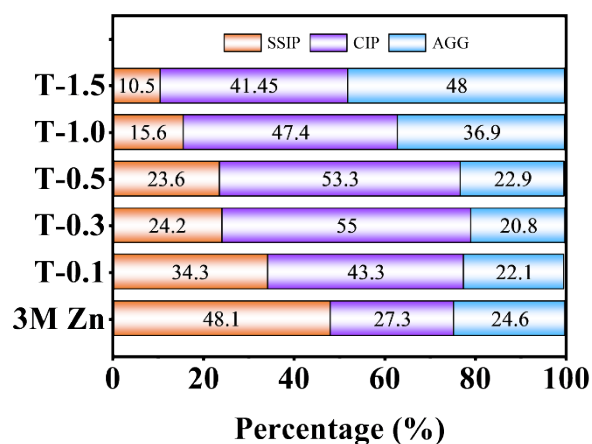


Fig.S16. Percentage of SSIPs/CIPs/AGGs for different electrolytes fitted by Raman peak area.

Table S5. Number of cations around an anion

		0.1	0.3	0.5	1.0	1.5	3 M Zn(OTf) ₂
SSIPs	0	180	300	280	320	320	2860
CIPs	1	240	1120	1090	1980	2930	2640
AGGs	2	40	180	300	1060	1750	500
	3	20			40	80	

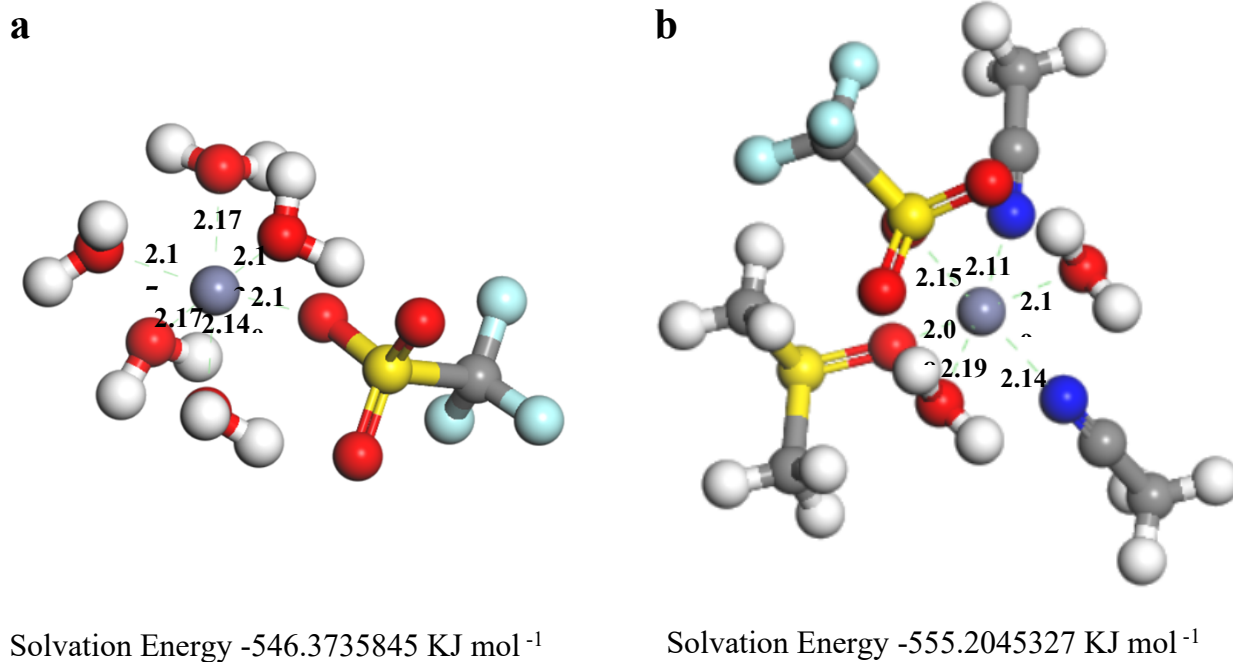


Fig.S17. Solvation structure model and solvation energy of 3 M $\text{Zn}(\text{OTf})_2$ and TSIS-0.3 electrolytes.

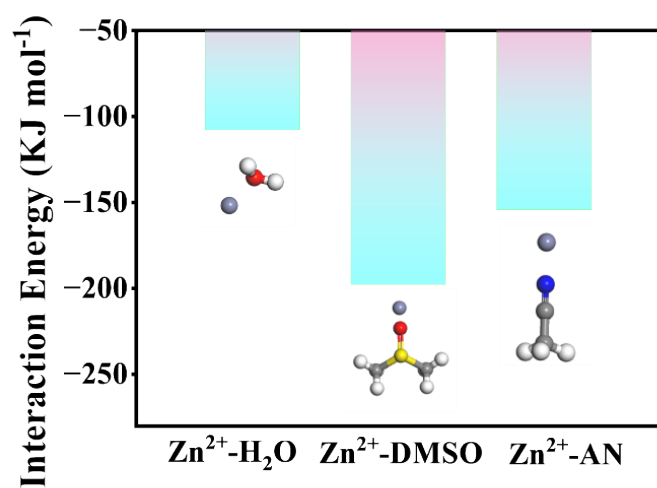


Fig.S18. The binding energy of $\text{Zn}^{2+}\text{-DMSO}$, $\text{Zn}^{2+}\text{-AN}$ and $\text{Zn}^{2+}\text{-H}_2\text{O}$ obtained from DFT calculations.

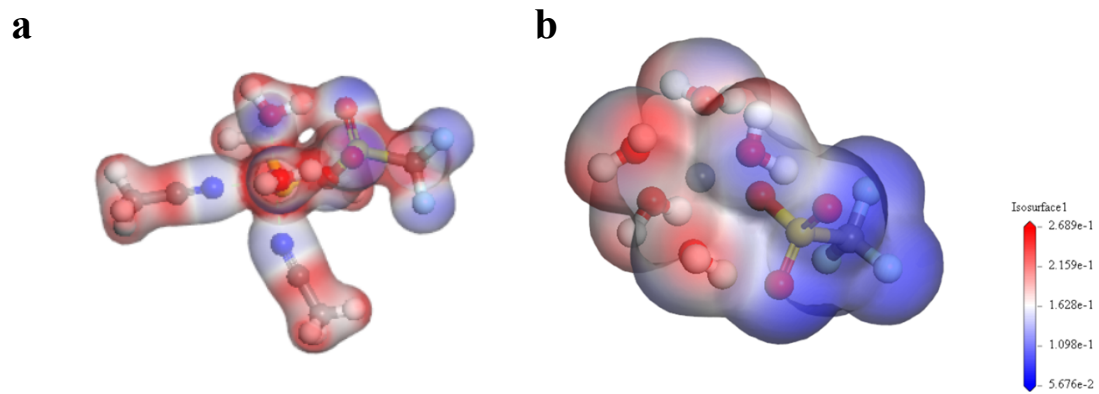


Fig.S19. Electrostatic potential maps of (a) $\text{Zn}(\text{H}_2\text{O})_2(\text{AN})_2(\text{DMSO})(\text{OTf})^+$ and (b) original $[\text{Zn}(\text{H}_2\text{O})_5(\text{OTf})]^+$ solvation structures.

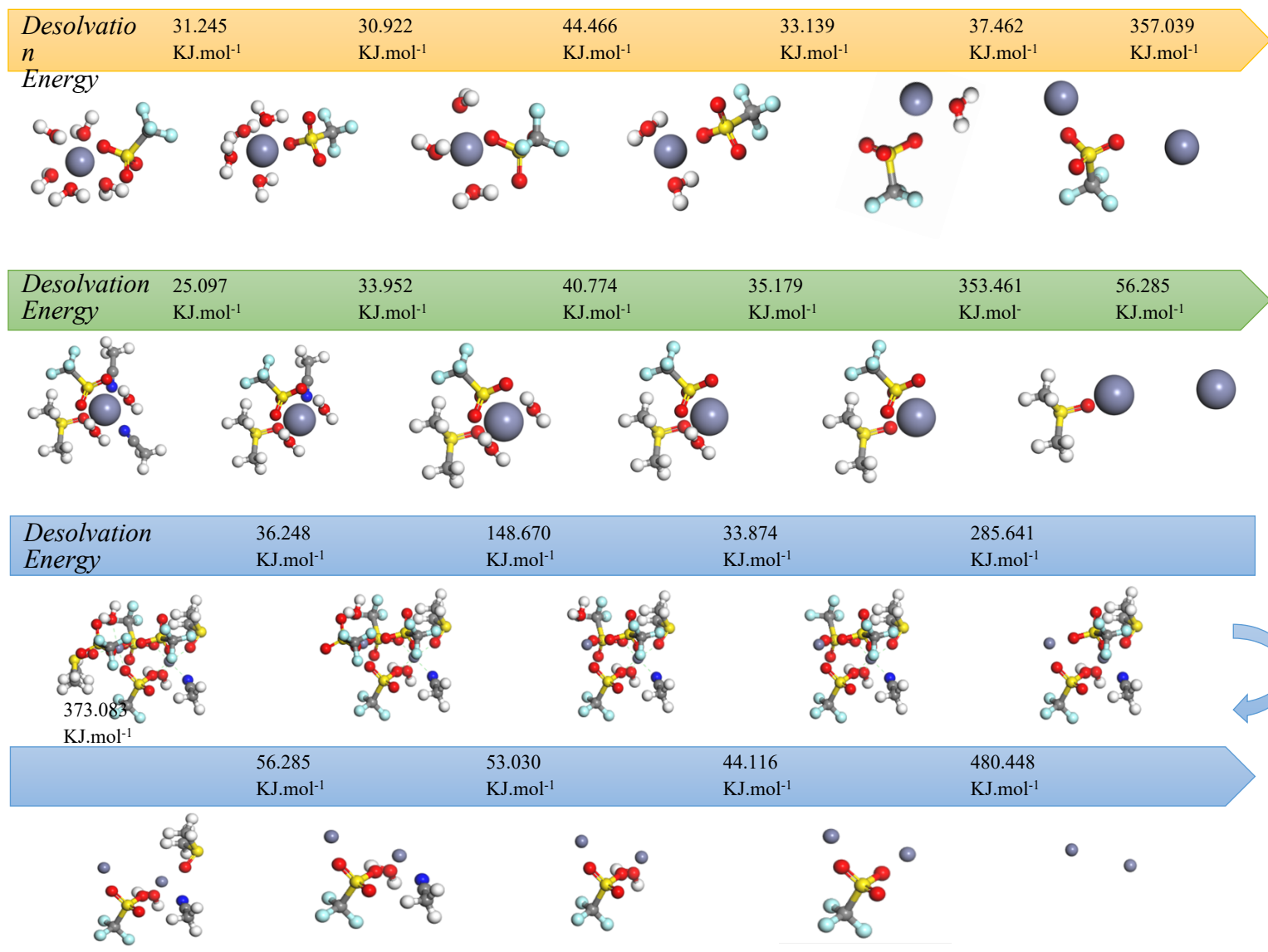


Fig.S20. Desolvation structure model and desolvation energy of CIP and AGG.

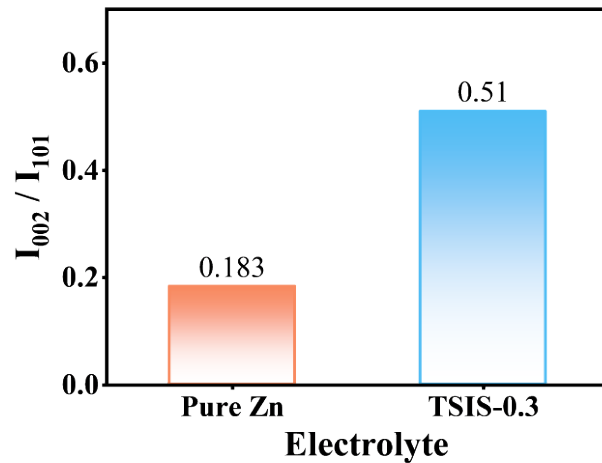


Fig.S21. The intensity ratio of Zn(002) to Zn(101) from the corresponding XRD results of Zn anode in 3 M Zn(OTf)₂ and TSIS-0.3 electrolytes.

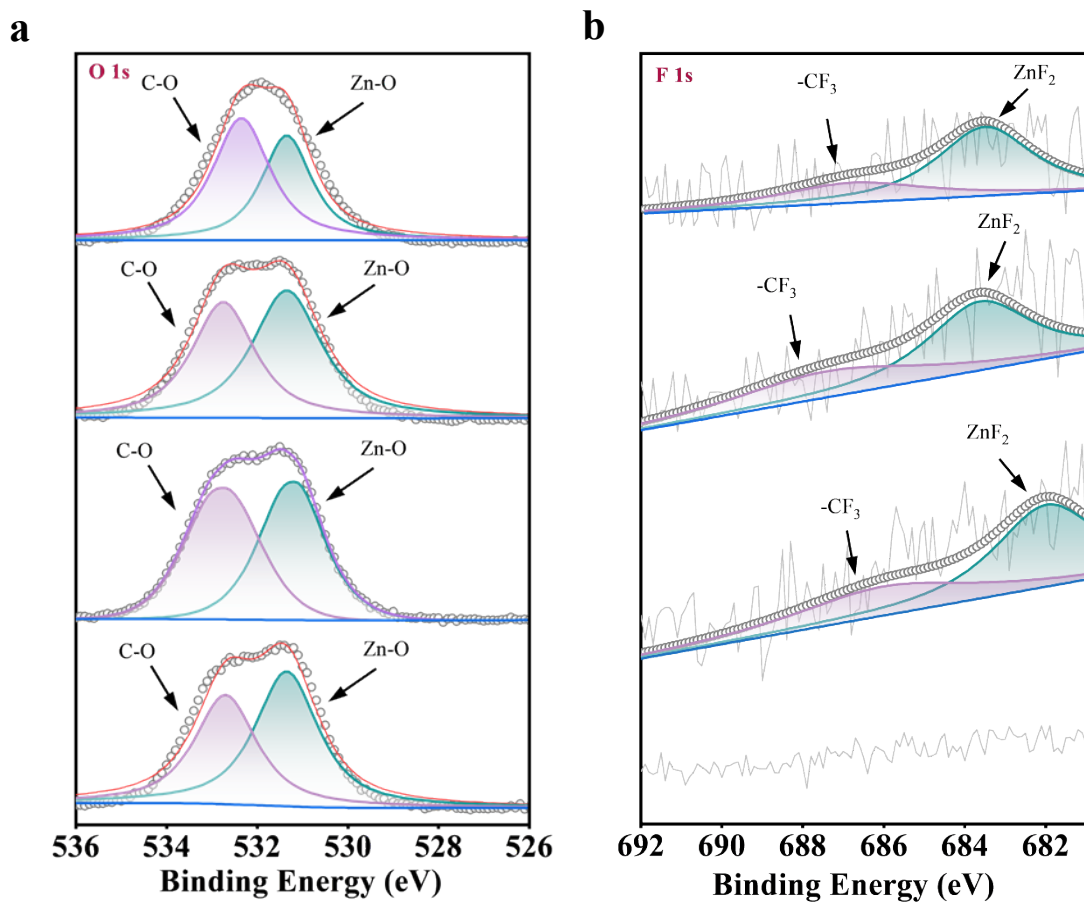


Fig.S22. XPS spectra of the (a) O 1s and (b) F 1s plated Zn top-most surface after 100 cycles with increasing sputtering time in the TIST-0.3.

Fig.S23. (a-d) The voltage profiles of the Zn||Zn symmetric cell tested in different electrolyte (TSIS-0.1, TSIS-0.5, TSIS-1.0, TSIS-1.5) at the current density of 1 mA cm^{-2} with the capacity of 1 mA h cm^{-2} .

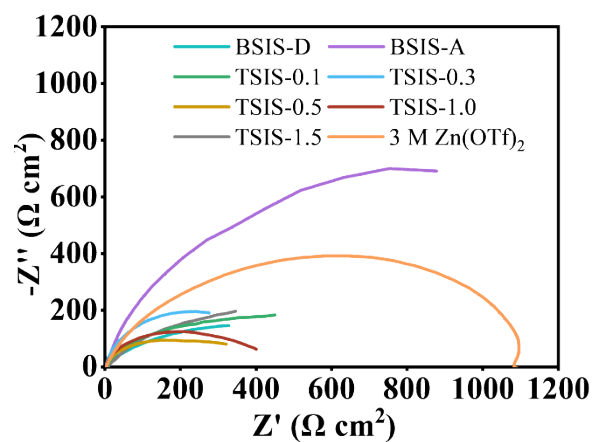


Fig.S24. The Nyquist plots of the symmetric cells at 3 M Zn(OTf)₂, TSIS-0.1, TSIS-0.3, TSIS-0.5, TSIS-1.0, TSIS-1.5, BSIS-D, BSIS-A electrolytes;

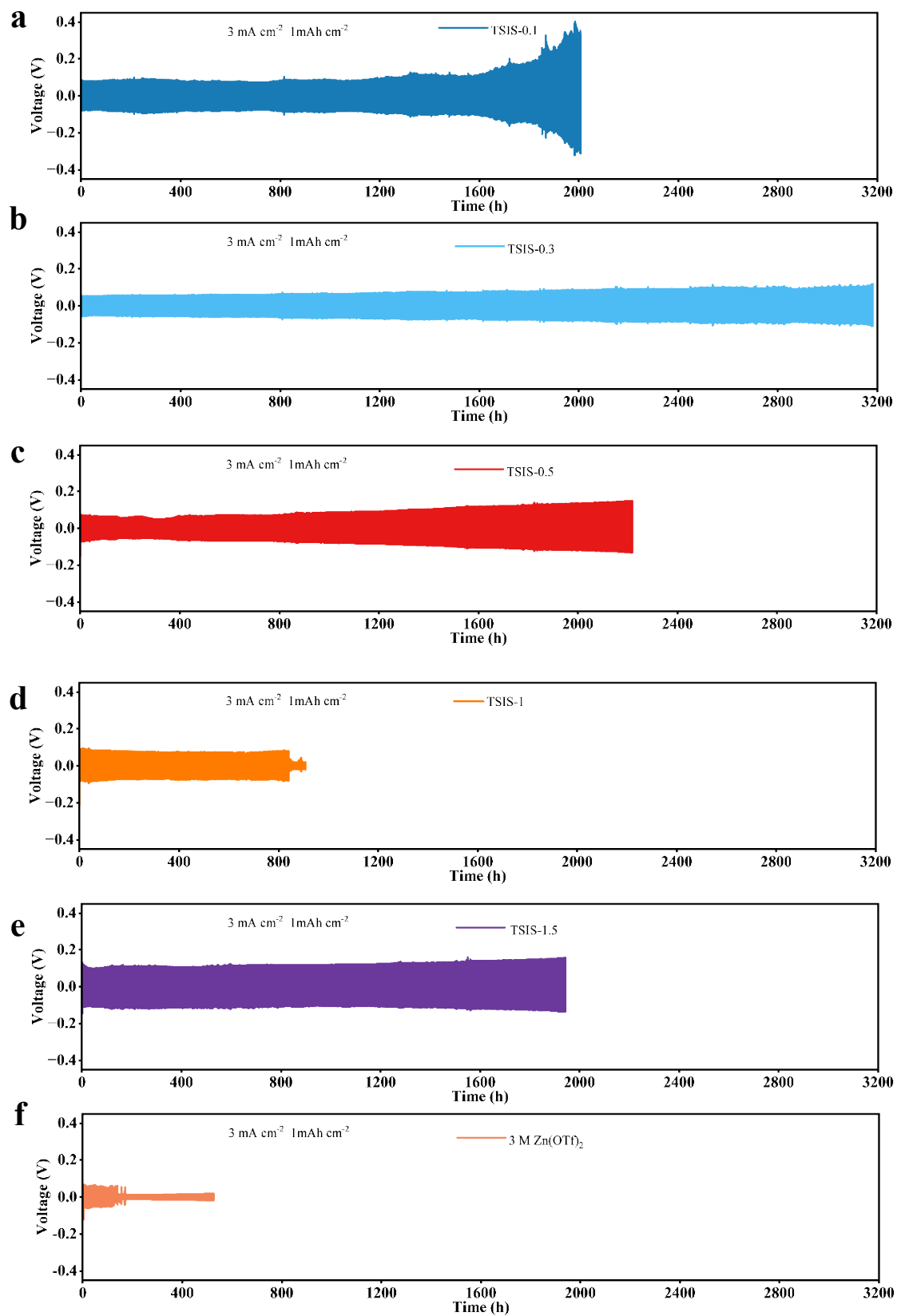


Fig.S25. (a-f) The voltage profiles of the Zn||Zn symmetric cell tested in different concentrations (TSIS-0.1, TSIS-0.3, TSIS-0.5, TSIS-1.0, TSIS-1.5, 3 M $\text{Zn}(\text{OTf})_2$) electrolyte at the current density of 3 mA cm^{-2} with the capacity of 1 mA h cm^{-2} .

Fig.S26. (a-d) At -20°C , the voltage profiles of the $\text{Zn}||\text{Zn}$ symmetric cell tested in different concentrations electrolyte (TSIS-0.1, TSIS-0.3, TSIS-0.5, TSIS-1.0, TSIS-1.5) at the current density of 0.5 mA cm^{-2} with the capacity of 0.5 mA h cm^{-2} .

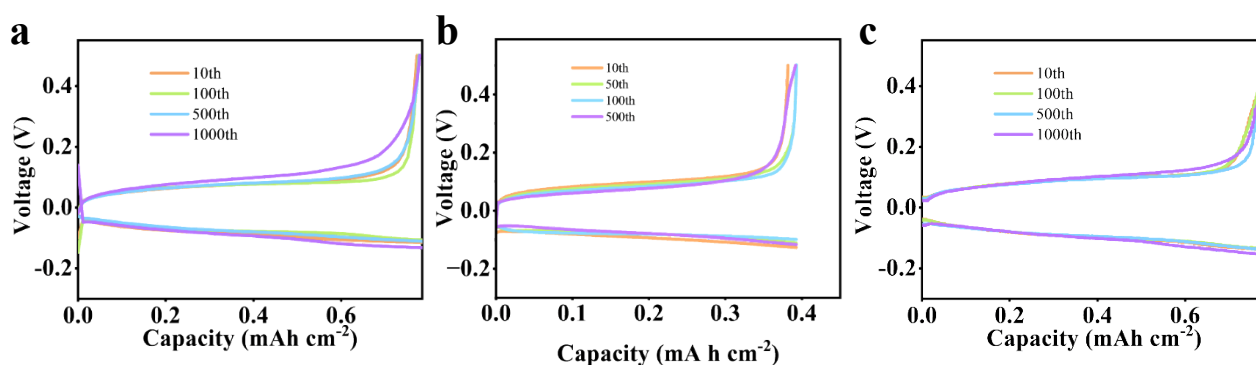


Fig.S27. (a) voltage-Capacity profiles of zinc plating/stripping at (a) 25°C, (b)–20 °C, and (c) 40 °C.

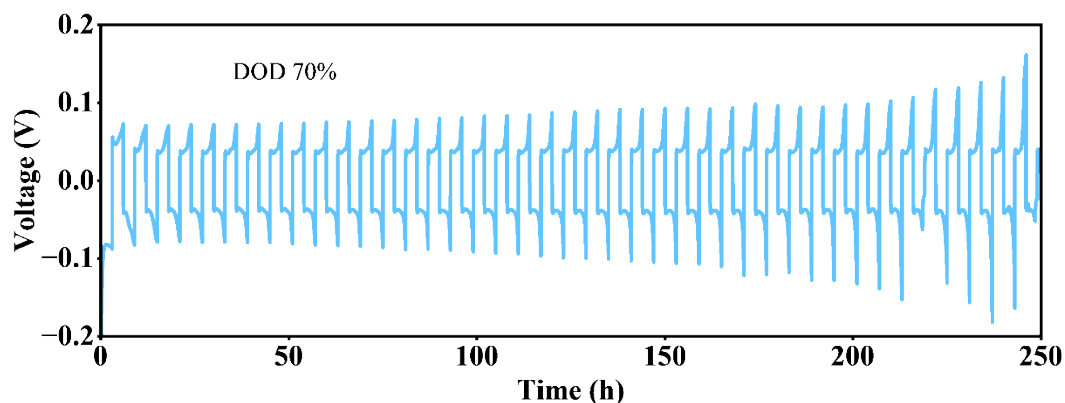


Fig. S28. Cycling stability of bare Zn||Zn symmetric cells with the TSIS-0.3 electrolyte at 2 mA cm⁻² with a capacity of 6 mA h cm⁻².

$$DOD = \frac{820mAh g^{-1} * 8.4 * 10^{-3}g}{0.78cm^2 * 2mAcm^{-2} * 3h} \approx 70\%$$

The Zn reversible cycle enables the battery to run steadily for about 250 hours without any noticeable irreversible voltage recorded, even at high rates of 2 mA cm⁻² and 6 mA h cm⁻².

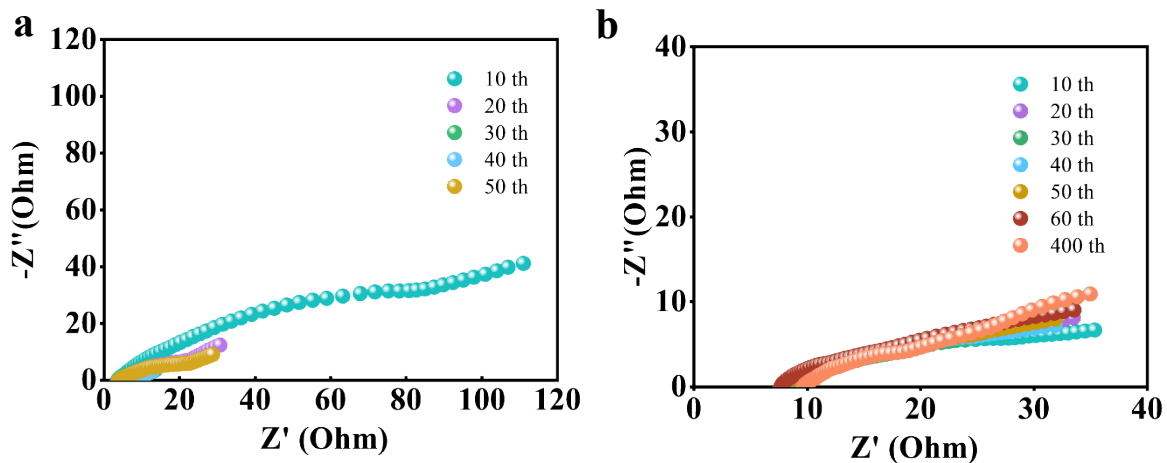


Fig.S29. EIS of 3 M Zn(OTf)₂ and TSIS-0.3 electrolytes.

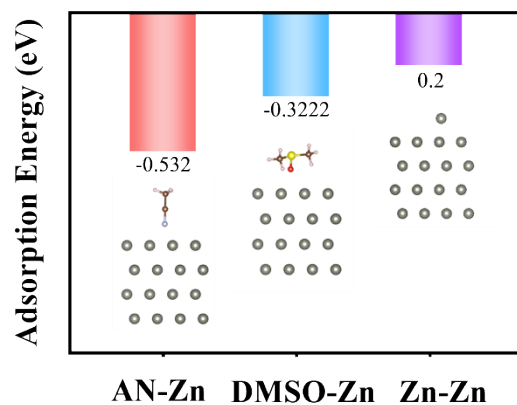


Fig.S30. Adsorption energy of AN, DMSO, Zn on the Zn (002) surface.

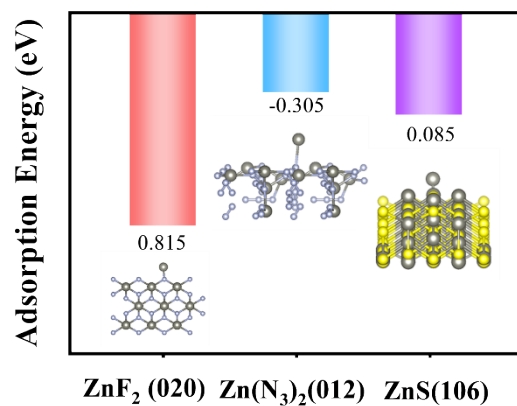


Fig.S31. Adsorption energy of Zn on the ZnF₂(020), Zn(N₃)₂(012), ZnS(106) surface.

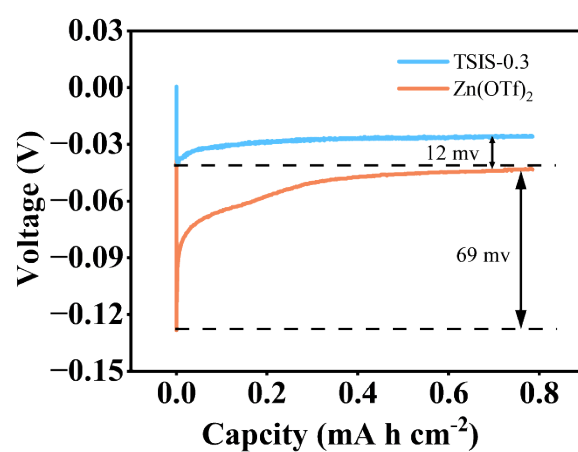


Fig.S32. Nucleation overpotentials in 3 M 3 M Zn(OTf)₂ and TSIS-0.3 electrolytes at 1st cycle.

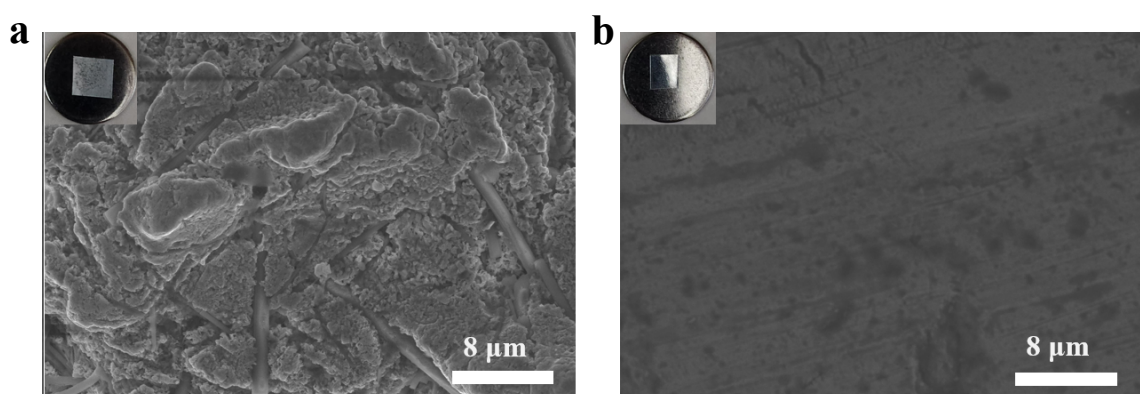


Fig.S33. Top-view SEM images of Zn||Zn symmetry cells after Chronoamperometry using TSIS-0.3 (a) 3 M Zn(OTf)₂,(b)

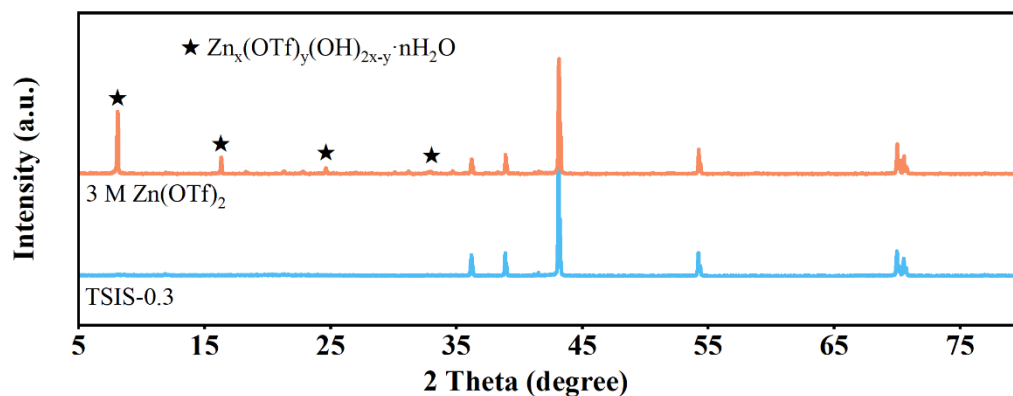


Fig.S34. XRD patterns of the Zn plate immersed in 3 M Zn(OTf)₂ and TSIS-0.3 electrolytes for 14 days.

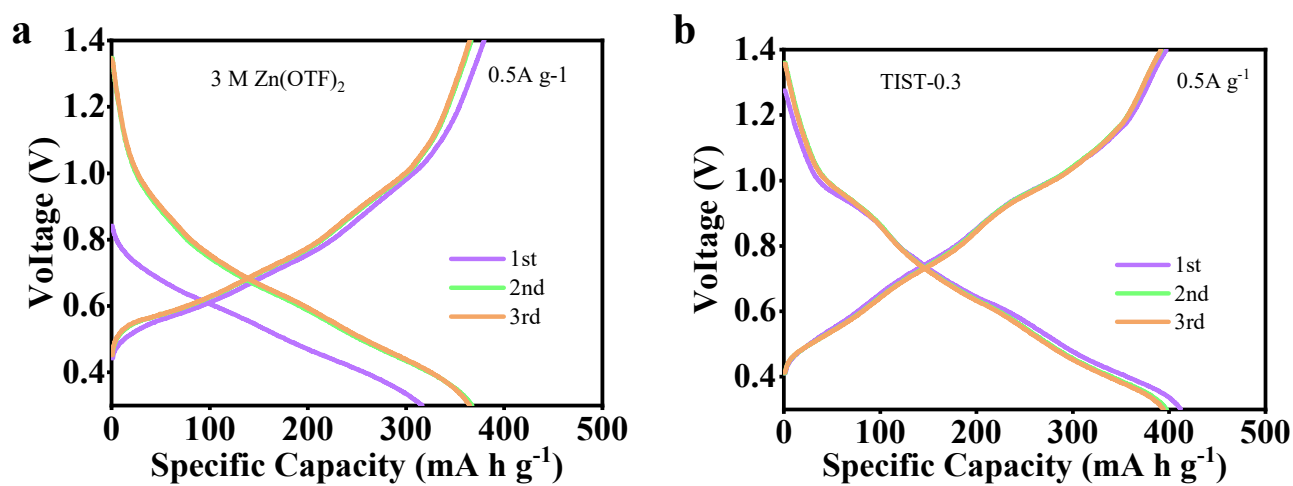


Fig.S35. Galvanostatic charge–discharge curves using 3 M Zn(OTf)₂ and TSIS-0.3 electrolytes at various current cycle.

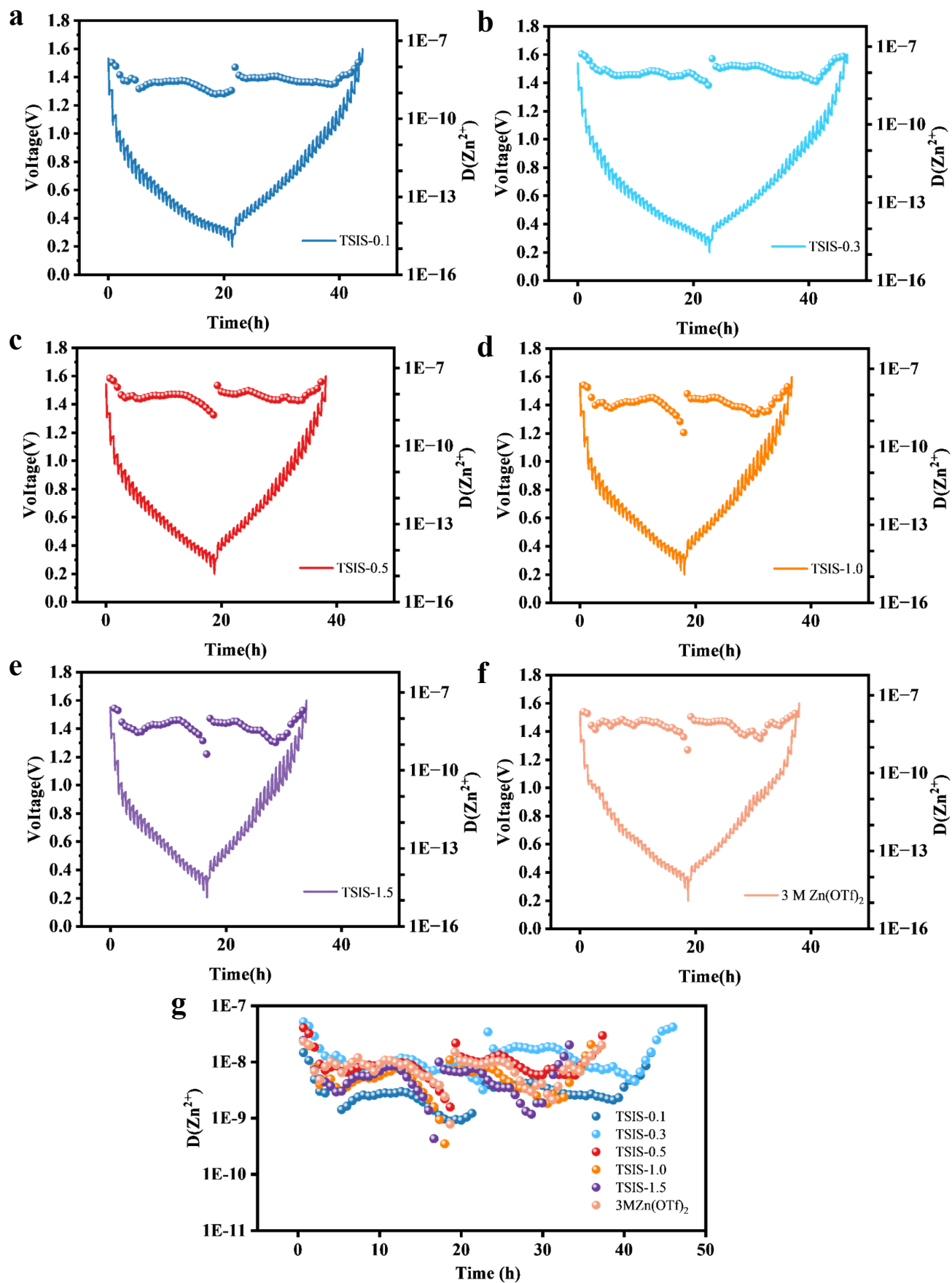


Fig. S36. (a-g) GITT curves and corresponding Zn^{2+} Diffusion coefficient.

Diffusion coefficients of Zn^{2+} in different electrolytes were evaluated using the galvanostatic intermittent titration technique (GITT). The diffusion coefficients of Zn^{2+} are marginally greater than those of the other electrolytes in the full cell utilizing the TSIS-0.3 electrolyte. The diffusion coefficients of Zn exhibit more stability, indicating that Zn^{2+} possesses rapid and stable transport capabilities in the TSIS-0.3 electrolyte ¹².

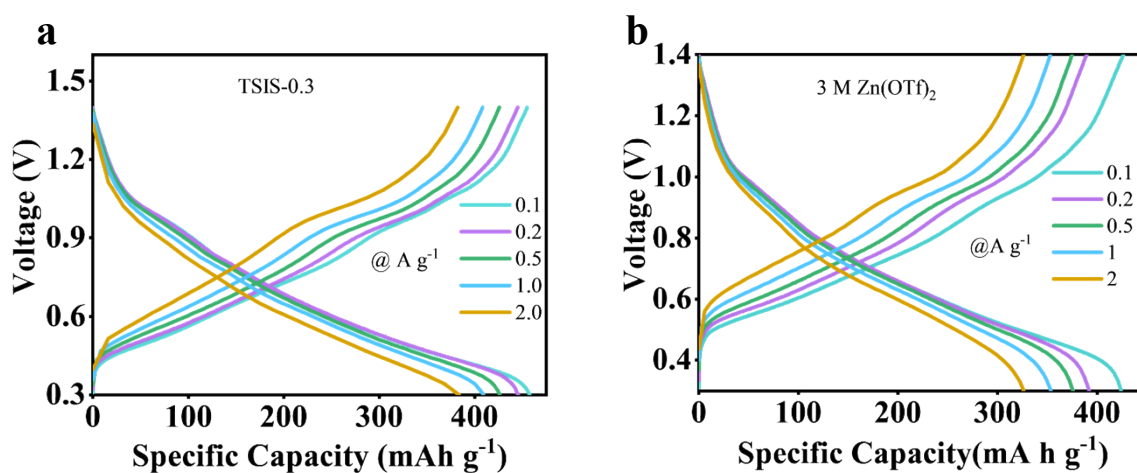


Fig.S37. Galvanostatic charge–discharge curves using 3 M Zn(OTf)₂ and TSIS-0.3 electrolytes at various current cycle.

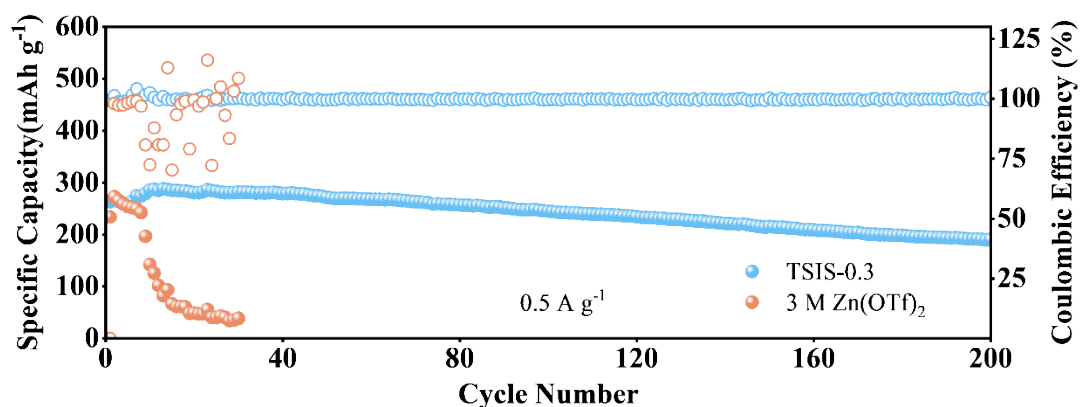


Fig. S38. Cycling stability of a Zn||V₆O₁₃ pouch cell operated at 0.5 A g⁻¹.

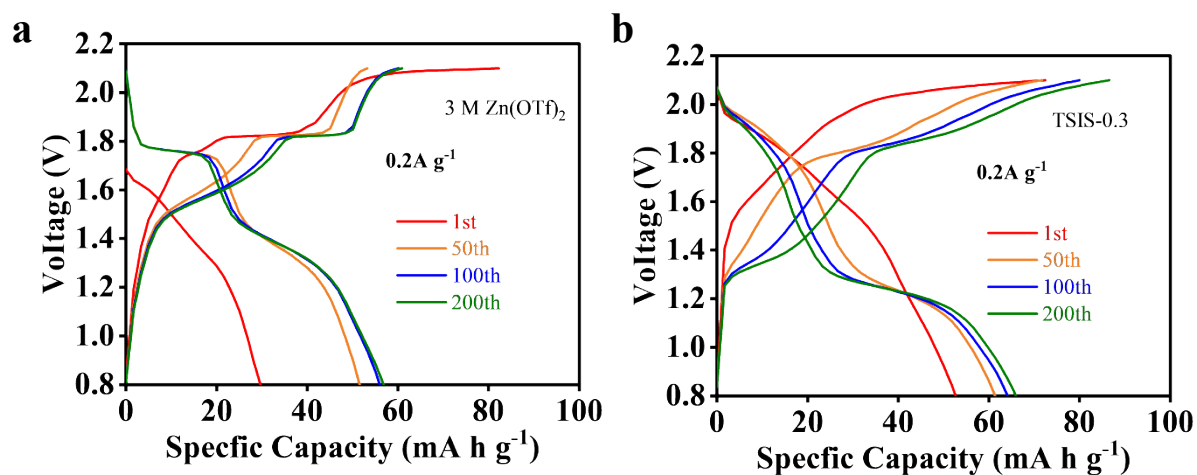


Fig.S39. Galvanostatic charge–discharge curves using 3 M Zn(OTf)₂ and TSIS-0.3 electrolytes at various current cycle.

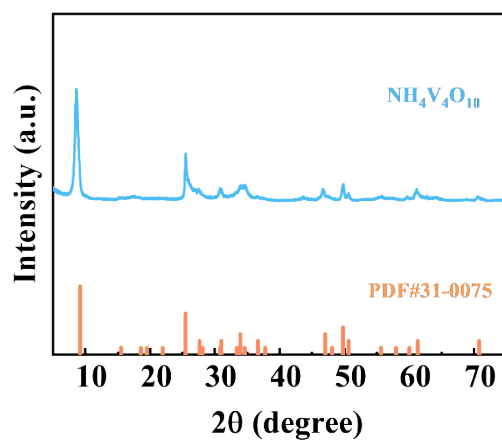


Fig. S40. XRD pattern of NH₄V₄O₁₀.

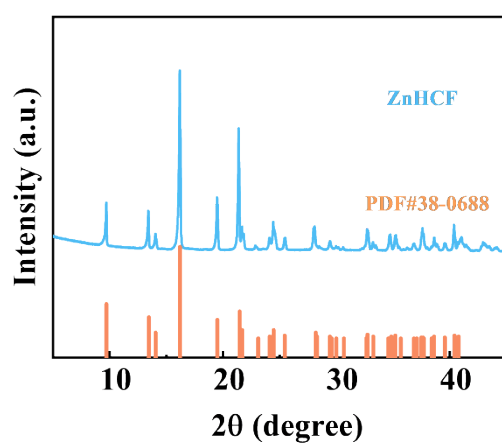


Fig. S41. The XRD pattern of ZnHCF.

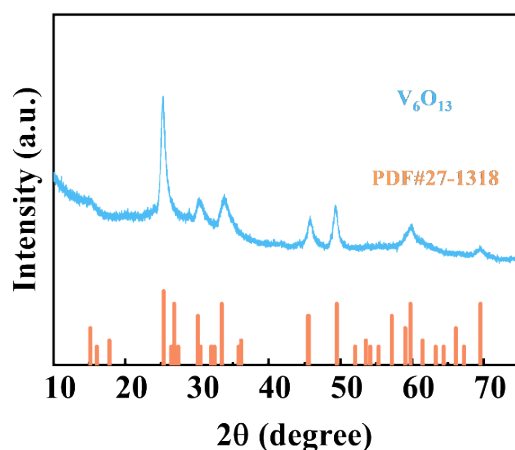


Fig. S42.The XRD pattern of V_6O_{13} .

Reference

1. F. Ming, Y. Zhu, G. Huang, A.-H. Emwas, H. Liang, Y. Cui and H. N. Alshareef, *Journal of the American Chemical Society*, 2022, **144**, 7160-7170.
2. T. Lv, G. Zhu, S. Dong, Q. Kong, Y. Peng, S. Jiang, G. Zhang, Z. Yang, S. Yang and X. Dong, *Angewandte Chemie*, 2023, **135**, e202216089.
3. T. Zhao, G. Xu, S. Yuan, Y. Chen and H. Yan, *The Journal of Physical Chemistry B*, 2010, **114**, 5025-5033.
4. R. Yuan, Y. Li, C. Li, H. Fang and W. Wang, *Colloids and Surfaces A: Physicochemical and Engineering Aspects*, 2013, **434**, 16-24.
5. S.-Y. Sun, X.-Y. Nie, J. Huang and J.-G. Yu, *Journal of Membrane Science*, 2020, **595**, 117528.
6. L. E. Camacho-Forero and P. B. Balbuena, *Chemistry of Materials*, 2019, **32**, 360-373.
7. L. Hector Jr, J. Herbst, W. Wolf, P. Saxe and G. Kresse, *Physical Review B—Condensed Matter and Materials Physics*, 2007, **76**, 014121.
8. G. Kresse and J. Furthmüller, *Physical review B*, 1996, **54**, 11169.
9. P. E. Blochl, *Physical Review-Section B-Condensed Matter*, 1994, **50**, 17953-17979.
10. A. Heyden, A. T. Bell and F. J. Keil, *The Journal of chemical physics*, 2005, **123**.
11. R. Yadav and P. S. Fedkiw, *Journal of the Electrochemical Society*, 2012, **159**, B340.
12. Z. Wang, P. Cui, X. Wang, M. Chang, Y. Yu, J. You, F. Hu, Y. Wu and K. Zhu, *Advanced Functional Materials*, 2024, 2407925.